ILASS Europe 2022

Far-Field Primary and Secondary Atomization Characteristics of External Mixing Sonic Twin-Fluid Atomizers

Raghav Sikka*[1], Knut Vågsæther[1], Dag Bjerketvedt[1] , Joachim Lundberg[1]
[1]Faculty of Technology, Natural Sciences, and Maritime Sciences
University of South-Eastern Norway, Porsgrunn, Norway
*Corresponding author email: raghav.sikka@usn.no

Abstract

This study investigated the 280 µm thick annular sheet far-field primary and secondary atomization spray characteristics with two different air-assisting configurations− converging-diverging (CD) and converging atomizers. The difference in airflow dynamics results in distinct sheet breakup and spray formation dynamics. The airflow rates range from 10-60 kg/h, and water flow rates range from 100–300 kg/h. High-speed ND: YAG laser-based imaging exhibited further ligament/fragments spread with a wider spray core in the CD atomizers due to the more prominent bursting effect. Particle density patterns depicted the cloud of newly formed droplets for all atomizers for a 200 kg/h liquid flow rate with different airflow rates. The mist formation occurs more in the CD atomizer as the stripping mechanism is more pronounced due to the highly intense air-liquid interaction owing to high contact strength. Shadowgraphy Imaging was performed for spray drop size measurements. The drop size distribution (DSD) and cumulative distribution curve were plotted at a 550 mm location downstream. It was observed that DSD was relatively more skewed towards smaller droplet sizes for CD atomizers. Sauter mean diameter (SMD) was plotted against radial locations for all atomizers. It was found that the SMD is minimum at the spray axis increases with an increase in radial locations. SMD value decreases with increased air-to-liquid ratio (ALR) for all atomizers employed with relatively smaller diameters for CD atomizer configuration due to the high aerodynamic momentum transfer to the liquid fragments.

Keywords
Air-assist atomizer, Spray dynamics, Shadowgraphy, Drop parameters, High-speed flows

Introduction

Twin-fluid atomization is the most widely used to atomize highly viscous fluids efficiently. There are numerous types of twin-fluid atomizers such as air-assist, Y-jet and effervescent atomizers that are mainly studied. Air-assist atomizers are more effective when used with liquid sheets than jets [1]. The merit of using air in atomizing liquid fuels lies in its contribution toward low pollutant emissions and improved combustion efficiency [2]. Due to the axisymmetric configuration, annular sheet-based atomizers with atomizing air are studied practically [3] [4]. Inner air configuration proved to be more effective in primary sheet disintegration with annular sheets [5] [6]. Sheet breakup happens either due to K-H instability (sinusoidal) or rupturing instability (non-sinusoidal) [7]. The primary instabilities play a major role in determining mean drop size and drop size distribution (DSD), as mentioned in [8]. Earlier studies were conducted without taking into consideration the air-assisting mechanism. [9],[10] studied the effect of shock dynamics by using sonic/supersonic air jets on liquid sheet disintegration. Mean drop

size (SMD) decreased with the advent of shocks; it still questions the usage of supersonic air jets for atomization. The coaxial liquid jet exposed to 1.5 Mach airflow was studied [11]. The irregular pressure distribution caused due to the waves pattern dictates the aerodynamic interaction at the interface boundary. Liquid metal atomization was investigated for convergent and converging-diverging close-coupled nozzles [12]. The long narrow supersonic air-jet producing finer particles while high dynamic pressure give narrow DSD. [13] while characterizing the annular sheet spray with an external sonic airflow, found relatively smaller drop size at the centre emphasizing the importance of high energy air-liquid interaction for tailoring the drop size range. The effect of De–Laval type nozzle geometry for atomizing air core on DSD was demonstrated [14]. Drop sizes and DSD are less affected by structural parameters at higher gas-to-liquid ratio (GLR); however, at lower GLR, smaller throat (exit) diameters and a moderate air-liquid distance provide optimal DSD. The objective of this study is to investigate the far-field spray formation dynamics and spray parameters based on droplet size measurements for different external mixing atomizer configurations involved. It was conjectured that dissimilarity in the near-nozzle air-liquid interaction would result in a different ligaments/droplets formation dynamics.

Materials & Methods

The nozzle consists of an internal cavity through which core air flows. 280 µm annular sheet thickness was obtained through a top attached. Two different atomizers: converging and converging-diverging (CD), were utilized with different orifice/throat diameters (D) (2.0 mm, 4.0 mm, and 5.0 mm), as shown in **Figure 1**. The diameter at the outlet in different CD atomizers is 6.0 mm. Airflow patterns were obtained through high-speed Shadow Imaging mentioned in detail [15]. Airflow rates varied from 10 kg/hr to 60 kg/h depending on the atomizer configuration. The mildly over-expanded flow leads to oblique shock waves in the CD atomizer. The Prandtl-Meyer expansion waves due to underexpanded flow formed in the converging atomizer **(Figure 2)**.

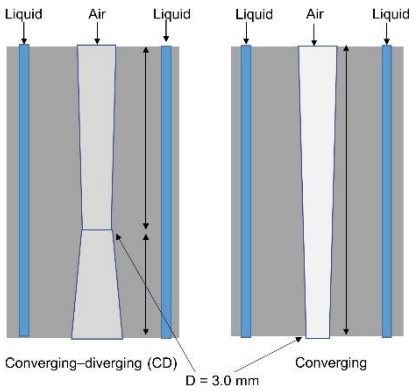

Figure 1. Schematic of both CD and converging atomizer geometry.

The laser-based high-speed imaging setup was adopted to obtain features of the far-field spray formation dynamics (schematically shown in **Figure 3**). The region was illuminated with the ND: YAG laser and the high-speed CMOS camera (Photron SA-Z). A 200 mm Nikon Micro lens with an f/5.6 aperture setting was used to obtain a field of view (FOV) of 120 mm x 125 mm with a camera resolution of ~8.36 pixel/mm. The images were recorded at 10 kHz with an exposure time limited by the laser. Liquid flow rates (range from 100 – 300 kg/h) were regulated by altering pump frequency, whereas compressed air was drawn from an in-house compressor (7.0 bar (g) maximum). The Coriolis type flowmeter was used for air and water flow rate measurements. The onset of liquid sheet interaction with either shock or expansion waves

dictates the annular sheet breakup; thus, ligaments structure during the spray formation. Spray characteristics such as Sauter mean diameter (SMD), droplet number density (DND) and drop size distribution (DSD) are dependent on the air-liquid interaction intensity.

The ParticleMaster package in Davis software (LaVision) was incorporated for the drop size measurements. The ND: YAG laser and high-speed camera attached with a Barlow lens (1.5x zoom) were used as shown in the schematic **(Figure 3)**. A 1024x1024 pixel image was obtained to render a magnified field of view (FOV) of 12.45 mm x 12.45 mm with a camera resolution of ~82.24 pixel/mm. The depth of field (DOF) calibration was performed using a calibration plate (50-1000 µm dark spots). Assuming axisymmetric spray, the measurements were taken for the left half, at one axial and three radial locations at 550 mm downstream, employing various fluid flow rates. 1000 images were taken at 1kHz to ensure sufficient accuracy in drop size calculations. Experiments were duplicated for a few cases to check the drop size measurements uncertainties, which were negligible (< 1%).

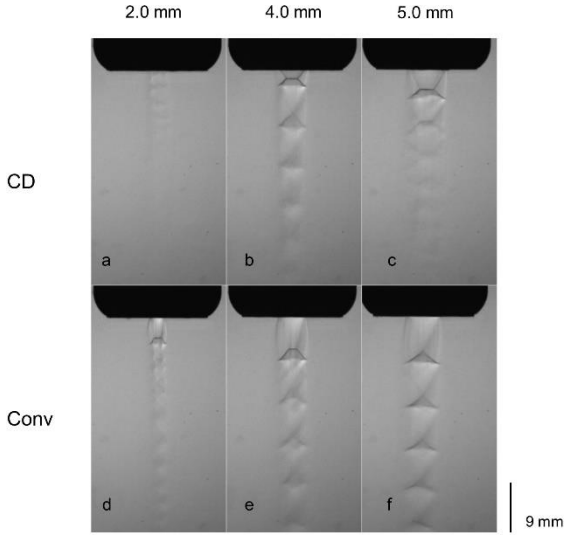

Figure 2. Shadowgraph Imaging with a) & d) 20 kg/h (2.0 mm), b) & e) 30 kg/h (4.0mm) and c) & f) 40 kg/h (5.0mm) airflow rates, respectively.

Experimental Results and Discussion

The far-field spray formation region was studied with larger (FOV) images **(Figure 4)**. The annular sheet breakup shows a similar disintegration mechanism as a bulk liquid jet. Due to the pressure distribution and surface tension effect, the annular jet converges to form the neck region downstream. The sheet develops perforations/holes on the periphery, especially in the CD atomizer. The bursting effect was observed in the neck region, which is more pronounced in the CD atomizer, also mentioned in [15]. The pulsations caused due to the bursting phenomenon at the neck region result in the spread of the newly formed ligaments. After disintegration, the perforated sheet leads to a larger spray spread with a wider dense spray core in the CD atomizer, resulting in a large fraction of ligaments. In contrast, sheet breakup results in a smaller spray spread with a narrower spray core in the converging atomizer.

The density of the spray core region depicts the magnitude of air-liquid interaction at the spray downstream. The nozzle diameter variation showed the multi-scale range of fragments formed in the CD atomizer, with relatively larger fragments formed in 2.0 mm diameter and smallest fragments in 5.0 mm diameter. The number and scale of fragments formed are dictated by the high contact strength of the air-jet, which depends on the dynamic pressure in the CD atomizer [10]. The scale of fragments size is comparable across all diameter configurations for the

converging atomizers. The droplet number density (DND) profiles (blue corresponds to dark region and red corresponds to bright region) in **Figure 5** depict the air-liquid interaction intensity through dense ligaments/droplets formation from the stripping mechanism. The wider spray core region, as discussed above, demonstrated the shearing effect of the high-speed airflow in the CD atomizer. The density of finer droplets increases as we move from 2.0 mm nozzle diameter to 5.0 mm nozzle diameter in both converging and CD atomizers, with more fine droplets formed in the CD atomizer configuration due to the increased velocity potential owing to the near-perfectly expanded flow.

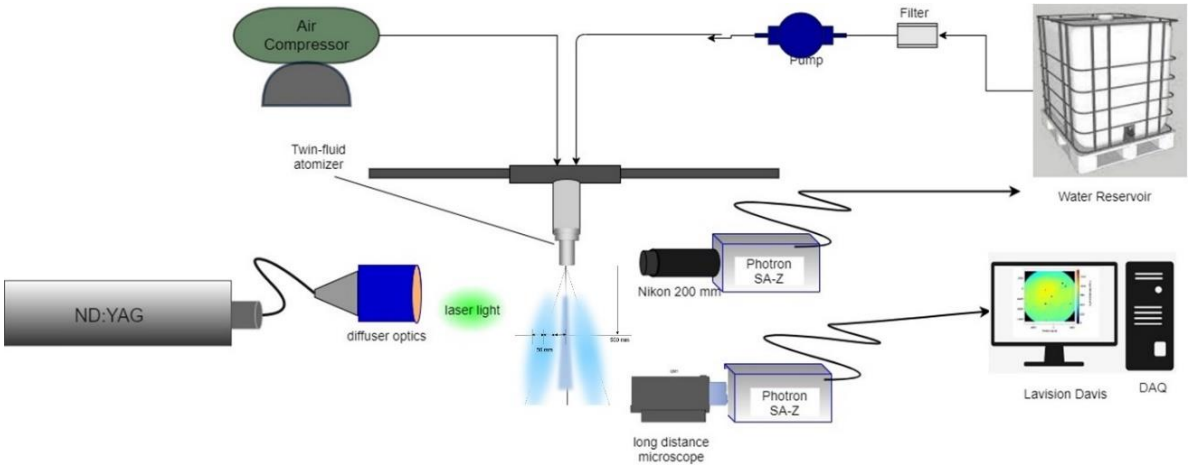

Figure 3. Schematic for shadowgraphy imaging for near-nozzle dynamics and drop size measurements.

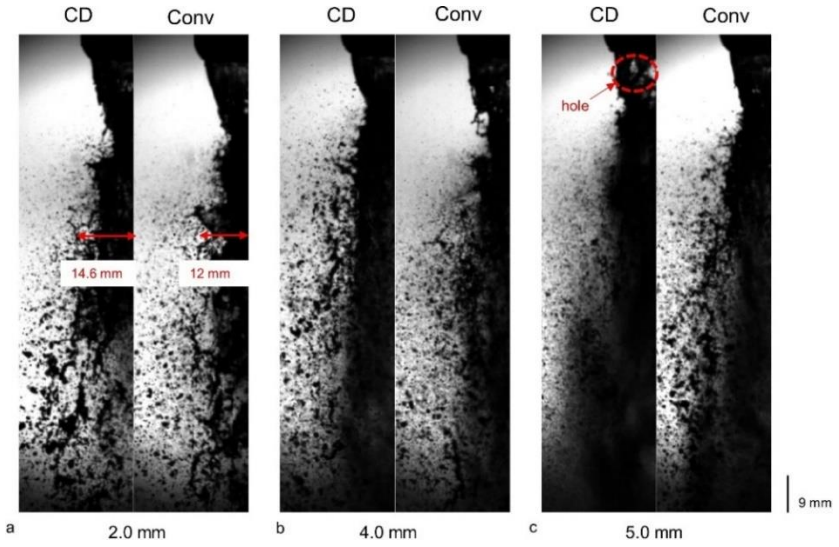

Figure 4. Imaging at 200kg/hr water flow rate with a) 10 kg/h (2.0 mm), b) 30 kg/h (4.0mm) and 40 kg/h (5.0mm) airflow rates.

DSD (normalized volume-based) and cumulative drop size distribution curve (in red) are plotted for 200 kg/h water flow rate in **Figure 6** for 550 mm axial location (spray centreline). DSD is uni-modal and non-axisymmetric as skewed towards the smaller droplets for all atomizer configurations. The DSD is more uniform (narrow) in CD atomizers than converging atomizers such that 80% of the droplet sizes by volume fall under ~200 μm for the former case, especially in 4.0 mm and 5.0 mm diameters. The narrower DSD in the 2.0 mm converging atomizer might be due to the less shock energy dissipation owing to narrow and long supersonic jet length formed [12].

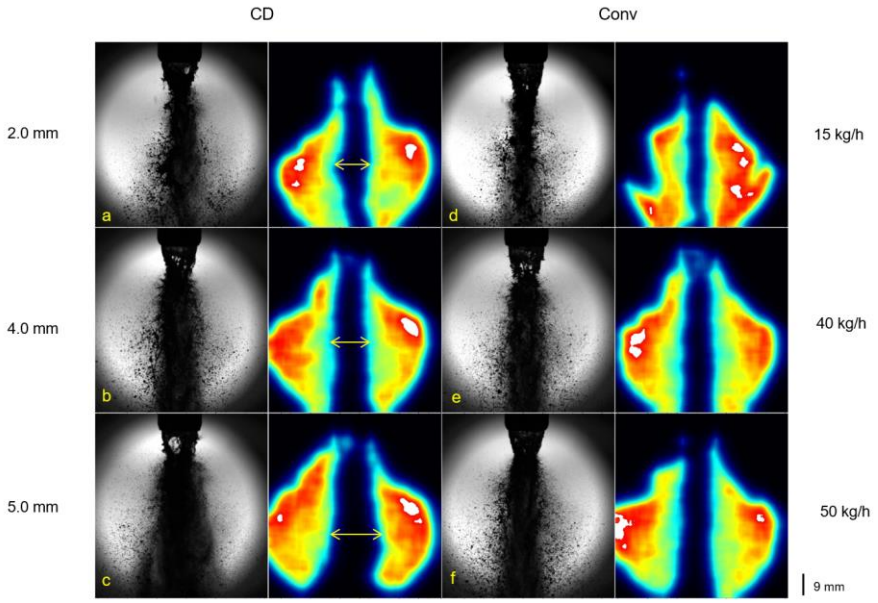

Figure 5. Raw Images and droplet number density profiles at 200 kg/h water flow rate for converging and CD atomizer.

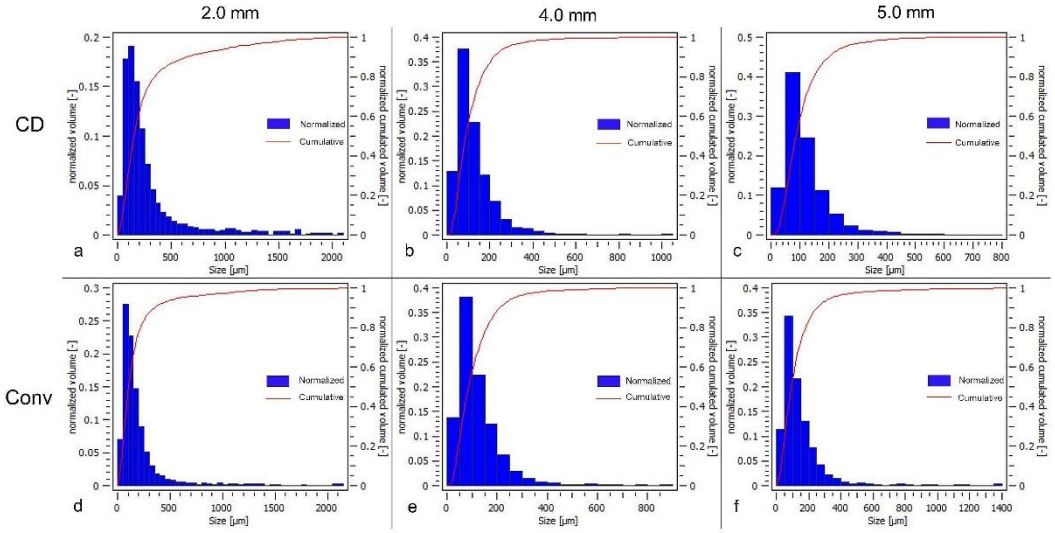

Figure 6. Histogram at 200 kg/h water flow rate for different airflow rates a) & d) 10 kg/h, b) & e) 30 kg/h and c) & f) 40 kg/h, at axial location 550 mm downstream (centerline).

In **Figure 7**, DSD and cumulative DSD curves (red) for a 200 kg/h water flow rate at a 150 mm radial location are shown. DSD is non-symmetric with reduced skewness towards the smaller droplets for all atomizer configurations, especially in the converging atomizers. The DSD is relatively more uniform in CD atomizers, such that the cumulative DSD span (80% of the droplet sizes by volume) fall under ~350 µm for a 5.0 mm diameter atomizer. DSD is generally wider in converging atomizers with a cumulative DSD span under ~550 µm for the 5.0 mm diameter atomizer due to the energy dissipated behind the normal shock wave caused by the shear-induced turbulence. On the contrary, the increased velocity potential in the far-field spray formation region in the CD atomizers results in uniform DSD [16]. In comparison, it reaches a much closer value in the case of the 2.0 mm atomizer. The cumulative DSD span falls under ~800 µm for converging and ~700 µm for CD atomizer for 2.0 mm diameter case due to the reason discussed above. The spray fluctuations leading to inhomogeneity forming droplet clusters dictate the spatial distribution (in volume) of the droplets [16].

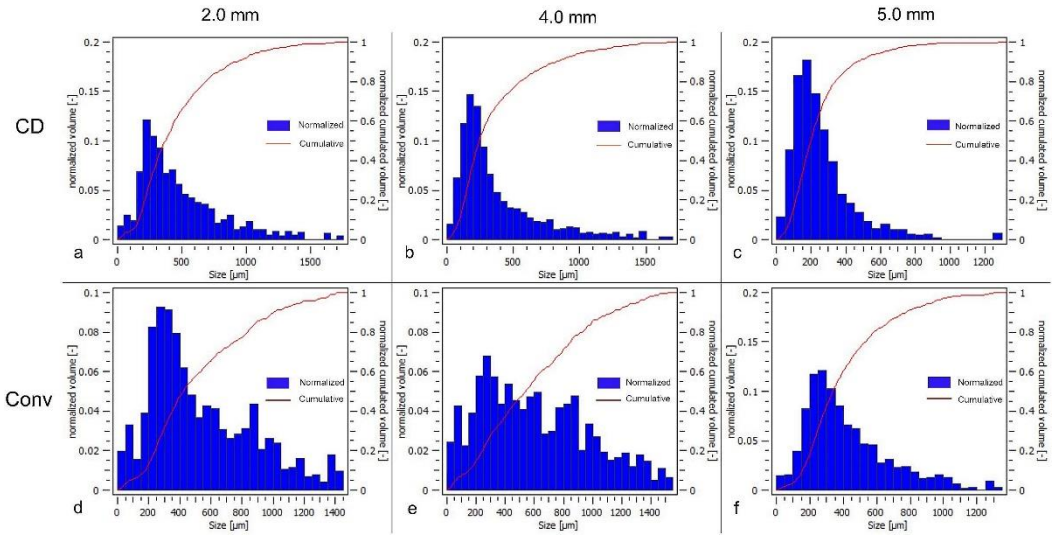

Figure 7. The histogram at 200 kg/h water flow rate for different airflow rates a) & d) 10 kg/h, b) & e) 30 kg/h and c) & f) 40 kg/h for radial location (150 mm) at 550 mm downstream.

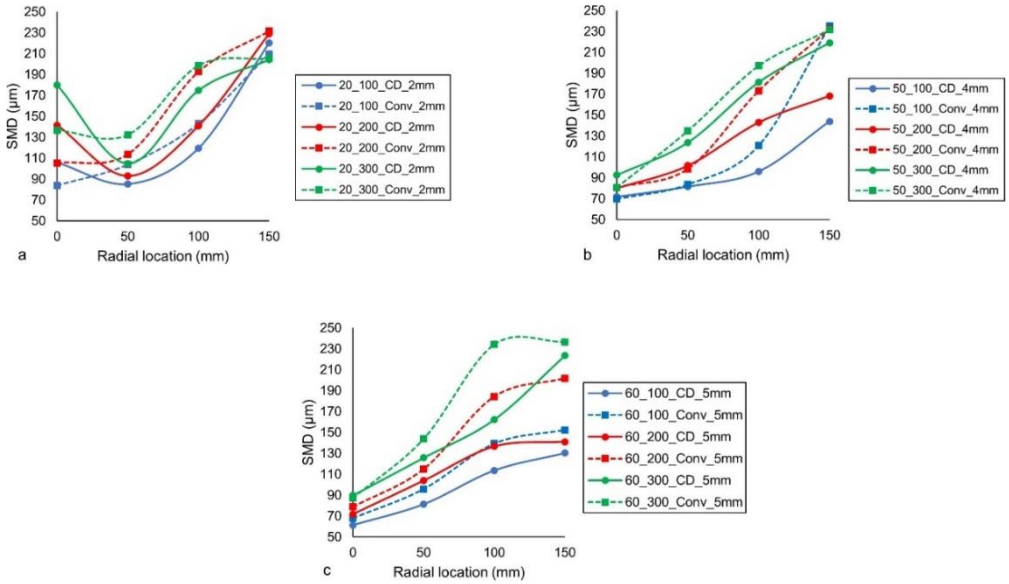

Figure 8. Plots showing SMD for airflow rates a) 20 kg/h, b) 50 kg/h and c) 60 kg/h, radial locations at 550 mm downstream from the exit.

The Sauter mean diameter (SMD) is plotted for different water flow rates at various radial locations at 550 mm axial location downstream **(Figure 8).** SMD was minimal at the spray axis location in 4.0 mm and 5.0 mm diameter atomizers. It increases with the increase in radial locations also observed in [17]. SMD slightly sink at 50 mm radial location then increases steeply with an increase in the radial locations for 2.0 mm diameter atomizer. The important point is that the maximum SMD (~240 µm) obtained at the 150 mm radial location is similar in all the atomizer configurations.

Sauter mean diameter (SMD) is plotted against various air-to-liquid mass ratios (ALR) at 550 mm downstream **(Figure 9).** SMD (D32) is relatively larger for the converging atomizers due to the air-jet dynamic pressure loss across shock waves, except in a 2.0 mm diameter atomizer where a long narrow supersonic jet aids in the droplet formation in both converging and CD configuration. The SMD follows an inverse relationship with ALR, with a more prominent decrement in the 5.0 mm atomizer case, which might be due to the higher ALR values

employed. A power curve fit depicts the SMD diminution with increased ALR values. The increment in ALR affects the mean drop size and drop size distribution such that narrower DSD and smaller SMD are observed at a higher ALR value [18].

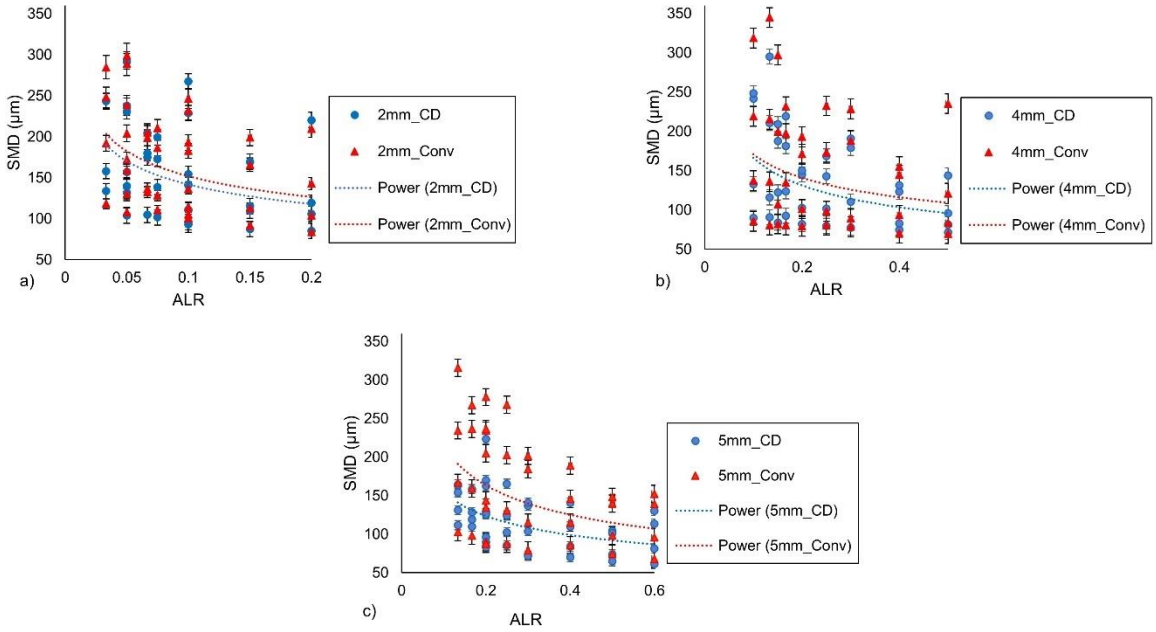

Figure 9. Plots showing SMD against air-to-liquid ratio (ALR) for radial locations at 550 mm downstream from the exit.

Conclusion

The spray characteristics of an annular sheet-based twin-fluid atomizer was studied using high-speed imaging and the Shadowgraphy technique. The breakup dynamics for the distinct airflow mechanism – the converging and the CD atomizer were analyzed. The wider spray core was observed for the CD atomizers in the spray formation region. The liquid stripping mechanism was observed from the periphery of the annular liquid; the effect is more pronounced in CD atomizers due to the high contact strength of the air jet resulting in spreading the newly-formed fragments/ligaments. The drop size distribution (DSD) is unimodal and skewed towards smaller droplets for both atomizers with narrower DSD for CD atomizers due to the intense interaction between air and liquid interfaces. DSD showed a comparable range in converging and CD atomizer for 2.0 mm diameter configuration, which might be less energy dissipation due to the narrow long supersonic jet. As compared to CD atomizers, larger droplet sizes are discerned for the converging atomizers configurations. The droplet size increases gradually with an increase in the radial location; the increment is slightly steeper in the larger diameter atomizers (4.0 mm and 5.0 mm). SMD follows an inverse relationship with ALR for all the atomizer configurations with higher values for converging atomizers due to the appositely mild air-liquid interaction owing to energy loss due to shear-induced turbulence.

Nomenclature

d	Air orifice (throat) diameter [mm]
t	Sheet thickness [µm]
Re_l	Liquid Reynolds number
Re_g	Air Reynolds number
ALR	Air-to-liquid mass ratio
U	Velocity [m·s^{-1}]

Greek symbols

μ	viscosity [Ns·m^{-2}]
ρ	density [kg·m^{-3}]
σ	surface tension [N·m^{-1}]

Acknowledgements

The researchers would like to express gratitude for the financial aid received from Wärtsilä Moss AS for the necessary equipment for the experimental setup.

References

[1] Balaji, K., Sivadas, V., Radhakrishna, V., Ashok Bhatija, K., and Sai Charan, K., 2018, "Experimental Characterization of Intrinsic Properties Associated With Air-Assisted Liquid Jet and Liquid Sheet," Journal of Fluids Engineering, **140**(5).

[2] Lefebvre, A., and Mcdonell, V., 2017, *Atomization and Sprays, Second Edition.*

[3] Leboucher, N., Laporte, G., and Carreau, J. L., 2007, "Effect of the Inner Gas Jet on Annular Liquid Sheet Atomization," 21st ILASS- Europe Meeting, pp. 1–5.

[4] Choi, C. J., and Lee, S. Y., 2005, "Drop Formation from a Thin Hollow Liquid Jet with a Core Air Flow," Atomization and Sprays, **15**, pp. 469–487.

[5] Fu, H., Li, X., Prociw, L. A., and Hu, T. C. J., 2003, "Experimental Investigation on the Breakup of Annular Liquid Sheets in Two Co-Flowing Airstreams," 1st International Energy Conversion Engineering Conference IECEC, (August), pp. 1–11.

[6] Leboucher, N., Roger, F., and Carreau, J. L., 2010, "Disintegration Process of an Annular Liquid Sheet Assisted by Coaxial Gaseous Coflow(S)," Atomization and Sprays, **20**(10), pp. 847–862.

[7] Duke, D., Honnery, D., and Soria, J., 2012, "Experimental Investigation of Nonlinear Instabilities in Annular Liquid Sheets," Journal of Fluid Mechanics, **691**, pp. 594–604.

[8] Sänger, A., Jakobs, T., Djordjevic, N., Kolb, T., and South, K. I. T. C., 2014, "Effect of Primary Instability of a High Viscous Liquid Jet on the Spray Quality Generated by a Twin-Fluid Atomizer," ILASS Europe, 26th Annual Conference on Liquid Atomization and Spray Systems, pp. 8–10.

[9] Kihm, K. D., and Chigier, N., 1991, "Effect of Shock Waves on Liquid Atomization of a Two-Dimensional Airblast Atomizer," Atomization and Sprays, **1**(1), pp. 113–136.

[10] Park, B. K., Lee, J. S., and Kihm, K. D., 1996, "Comparative Study of Twin-Fluid Atomization Using Sonic or Supersonic Gas Jets," Atomization and Sprays, **6**, pp. 285–304.

[11] Issac, K., Missoum, A., Drallmeier, J., and Johnston, A., 1994, "Atomization Experiments in a Coaxial Coflowing Mach 1.5 Flow," AIAA Journal, **32**(8), pp. 1640–1646.

[12] Mates, S. P., and Settles, G. S., 2005, "A Study of Liquid Metal Atomization Using Close-Coupled Nozzles , Part 2 : Atomization Behavior.," Atomization and Sprays, **15**(1), pp. 41–59.

[13] Marklund, M., and Engstr öm, F., 2010, "Water Spray Characterization of a Coaxial Air-Assisted Swirling Atomizer at Sonic Conditions," Atomization and Sprays, **20**(11), pp. 955–963.

[14] Chen, B., Gao, D., Li, Y., Chen, C., Yuan, X., Wang, Z., and Sun, P., 2020, "Investigation of the Droplet Characteristics and Size Distribution during the Collaborative Atomization Process of a Twin-Fluid Nozzle," International Journal of Advanced Manufacturing Technology, **107**(3–4), pp. 1625–1639.

[15] Sikka, R., Bjerketvedt, D., Lundberg, J., and Va, K., 2022, "Visualization Study of Annular Sheet Breakup Dynamics in Sonic Twin-Fluid Atomizers," Journal of Visualization.

[16] Fritsching, U., 2005, "Droplets and Particles in Sprays: Tailoring Particle Properties within Spray Processes," China Particuology, **3**(1–2), pp. 125–133.

[17] Li, X., and Shen, J., 2001, "Experiments on Annular Liquid Jet Breakup," Atomization and Sprays, **11**, pp. 557–573.

[18] Kulkarni, A. P., and Deshmukh, D., 2017, "SPATIAL DROP-SIZING IN AIRBLAST ATOMIZATION-AN EXPERIMENTAL STUDY," Atomization and Sprays, pp. 949–961.